

Cross-correlating the Microwave Sky with Galaxy Surveys

Pablo Fosalba^{1,2}, Enrique Gaztañaga^{3,4}, Francisco J Castander³

¹ *Institut d'Astrophysique de Paris, 98bis Bd Arago, 75014 Paris, France*

² *Institute for Astronomy, University of Hawaii, 2680, Woodlawn Drive, HI-96822, Honolulu, USA*

³ *Institut d'Estudis Espacials de Catalunya/CSIC, Gran Capità 2-4, 08034 Barcelona, Spain*

⁴ *INAOE, Astrofísica, Tonantzintla, Puebla 7200, Mexico*



We present results for the cross-correlation between the WMAP 1st-year cosmic microwave background (CMB) anisotropy data and optical galaxy surveys: the APM and SDSS DR1 catalogs. Our measurement of a positive CMB-galaxy correlation on large angles ($\theta > 4^\circ$) yields significant detections of the Integrated Sachs-Wolfe (ISW) effect and provides a new estimate of dark-energy in the universe, $\Omega_\Lambda = 0.69 - 0.86$ (2σ range). In addition, the correlated signal on small angles ($\theta < 1^\circ$) reveals the imprint left by hot intra-cluster gas in the CMB photons: the thermal Sunyaev-Zeldovich (SZ) effect.

1 Introduction

The pattern of primary temperature anisotropies of the cosmic microwave background (CMB) is expected to be distorted by the large-scale structures of the universe as microwave photons travel from the last scattering surface ($z \simeq 1100$) to us (see e.g.¹³). On large-scales (i.e, angular scales comparable to large clusters and super-clusters as seen in projection), the observationally favored flat Λ CDM models predict such distortion is mainly produced by the energy injection photons experience as they cross time-evolving dark-matter gravitational potential wells: the so-called integrated Sachs-Wolfe effect (ISW)^{21,15}. On smaller scales, the primary CMB anisotropy pattern is altered when primordial photons scatter off free electrons in the hot intra-cluster gas: the thermal Sunyaev-Zeldovich effect (SZ)²⁴.

Although these secondary anisotropies can be potentially measured from CMB maps alone, in practice the ISW detection is severely limited by primary CMB anisotropies and cosmic variance, whereas the SZ requires high-spatial resolution, multi-frequency observations and it is potentially contaminated by point sources. Alternatively, large-scale structure tracers, such as galaxy surveys, provide a unique window to probe the baryon and dark-matter distribution at

intermediate redshifts ($z \lesssim 2$) and its imprint in microwave photons without significant confusion from other cosmological signals^{5,19,20}. The combination of nearly full-sky high-sensitivity CMB maps obtained by WMAP³ with wide large-scale structure surveys has recently led to the first detections of the ISW effect, setting new constraints on the dark-energy content of the universe^{4,18}. It has also allowed probing the SZ effect with cluster templates^{6,10,17}.

Here we concentrate on the cross-correlation of the cosmic CMB anisotropies measured by WMAP with galaxy number count fluctuations in the APM Survey¹⁶ and the first data release of the Sloan Digital Sky Survey^{a 2} (SDSS DR1). Our CMB-galaxy correlation analyses find significant detections for both the integrated Sachs-Wolfe (ISW) and thermal Sunyaev-Zeldovich (SZ) effects. The reported ISW detection is in good agreement with previous analyses based on X-ray and radio sources^{4,18}. Further details on the results presented here are given in^{7,8}. A similar analysis using SDSS data was presented in²² while, more recently,¹ computed the CMB-galaxy correlation for 2MASS galaxies.

2 Data

We make use of the largest datasets currently available to study the CMB-galaxy cross-correlation. In order to probe the galaxy distribution, we have used the APM survey as well as selected subsamples from the SDSS DR1.

The APM Galaxy Survey is based on 185 UK IIIA-J Schmidt photographic plates each corresponding to $5.8 \times 5.8 \text{ deg}^2$ on the sky limited to $b_J \simeq 20.5$ and having a mean depth of $\simeq 400 \text{ Mpc/h}$ for $b < -40 \text{ deg}$ and $\delta < -20 \text{ deg}$. These fields were scanned by the APM machine and carefully matched using the $5.8 \times 0.8 \text{ deg}^2$ plate overlaps. Out of the APM Survey we considered a $17 < b_J < 20$ magnitude slice, which includes 1.2 million galaxies at a mean redshift $\bar{z} = 0.15$, in an equal-area projection pixel map with a resolution of $3.5'$, that covers over 4300 deg^2 around the SGC.

The SDSS DR1 survey covers $\sim 2000 \text{ deg}^2$ (i.e., 5 % of the sky). The samples we analyzed have different redshift distributions and a large number of galaxies (10^5 - 10^6 , depending on the sample). We concentrate our analysis on the North sky ($\sim 1500 \text{ deg}^2$, i.e., 3.6 % of the sky), because it contains the largest and wider strips. The South SDSS DR1 ($\sim 500 \text{ deg}^2$) consists of 3 narrow and disjoint 2.5° strips, which are less adequate for our analysis. Our main sample, hereafter *SDSS all*, includes all objects classified as galaxies with extinction corrected magnitude $r < 21$, and a low associated error ($< 20\%$). This sample contains ~ 5 million galaxies distributed over the North sky. Its predicted redshift distribution is broad and has a median redshift $\bar{z} \sim 0.3$. Our color selected high-redshift sample (*SDSS high-z* thereafter) comprises $\sim 3 \times 10^5$ galaxies, with $\bar{z} \sim 0.5$.

For the CMB data, we use the first-year full-sky WMAP maps³. We shall focus on the V-band ($\sim 61 \text{ GHz}$) as it conveniently combines low pixel noise and high spatial resolution, $21'$. In addition, we have also used the W-band and a foreground “cleaned” WMAP map²⁵ to check that our results are free from galactic contamination. We mask out pixels using the conservative Kp0 mask, that cuts out 21.4% of the sky³. All the maps used have been digitized into $7'$ pixels using HEALPix^{b 9}.

3 Cross-Correlation Estimation

We define the cross-correlation function as the expectation value of density fluctuations $\delta_G = N_G / \langle N_G \rangle - 1$ and temperature anisotropies $\Delta_T = T - T_0$ (in μK) at two positions $\hat{\mathbf{n}}_1$ and $\hat{\mathbf{n}}_2$ in the sky: $w_{TG}(\theta) \equiv \langle \Delta_T(\hat{\mathbf{n}}_1) \delta_G(\hat{\mathbf{n}}_2) \rangle$, where $\theta = |\hat{\mathbf{n}}_2 - \hat{\mathbf{n}}_1|$.

^a<http://www.sdss.org/dr1>

^b<http://www.eso.org/science/healpix>

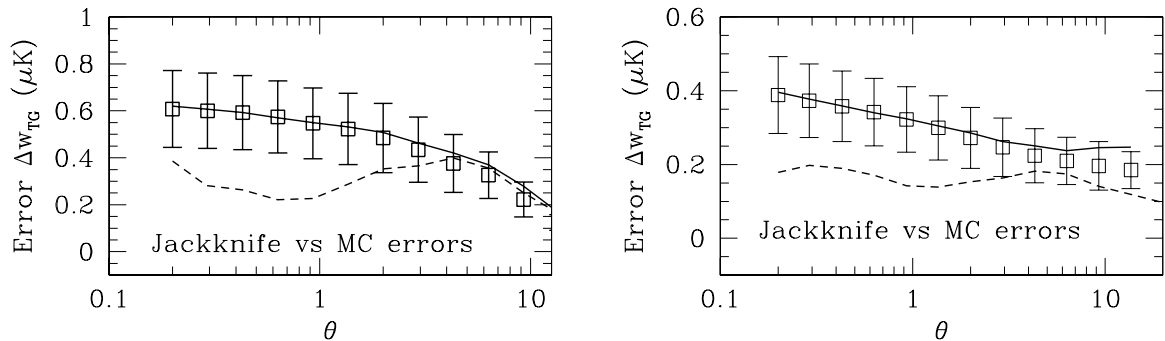


Figure 1: **(Left)** error estimation for the WMAP-APM; **(Right)** errors for the WMAP-SDSS. Solid line gives errors from the dispersion in 200 Monte-Carlo simulations; Squares with errorbars give the mean and dispersion in the jack-knife error estimation over the same simulations. Dashed lines show the jack-knife errors in the WMAP-Galaxy correlation for the real samples. Angular scales are given in degrees.

We compute the CMB-galaxy correlation and the associated statistical error-bars using the jack-knife (JK) method (see ⁷ and references therein for further details) The survey is divided into M separate regions the sky, each of equal area ($M = 8 - 16$ depending on the survey used; we find no significant differences as a function of M). The w_{TG} analysis is then performed M times, each time removing a different region, the so-called JK subsamples. The covariance C_{ij} for w_{TG} between scales θ_i and θ_j is obtained by re-scaling the covariance of the JK subsamples by a factor $M - 1$ To test the JK errors and their covariance we have also run 200 WMAP V-band Monte-Carlo (MC) realizations of the measured WMAP temperature angular power-spectrum³ and the white noise for the V-band estimated for 1 year of data ¹¹.

For each MC simulation we estimate the mean "accidental" correlation w_{TG} of simulated CMB maps to the SDSS galaxy density fluctuation map. We also estimate the associated JK error in each MC simulation. Fig. 1 compares error estimates for the APM (left panel) and SDSS (right) surveys. They show the 'true' sampling error from the dispersion of $w_{TG}(\theta)$ in 200 MC simulations, along with the mean and dispersion of the JK errors in the same simulations. The JK and MC errors agree within 10 – 20% for $\theta \gtrsim 5$ degrees, i.e, the scales relevant for the ISW effect (see below). The observed differences in error estimation, particularly on smaller scales, are not totally surprising as the MC simulations do not include any physical correlations and use a CMB power spectrum that is valid for the whole sky, and not constraint as to match the CMB power over the region covered by the galaxy survey. Actually, the JK errors provide a model free estimation that is only subject to moderate (20%) uncertainty, while MC errors depend crucially on the model assumptions that go into the simulations.

Fig.2 shows the CMB-galaxy correlation w_{TG} for the APM (left) and SDSS (right) catalogs together with the corresponding JK error. We derive the significance of the detected correlation taking into account the large (JK) covariance between neighboring (logarithmic) angular bins in survey sub-samples. To assign a conservative significance for the detection (i.e. against $w_{TG} = 0$) we estimate the minimum χ^2 fit for a constant w_{TG} and give the difference $\Delta\chi^2$ to the $w_{TG} = 0$ null detection. For example, at scales $\theta = 4 - 10^\circ$ we get: $w_{TG} = 0.35 \pm 0.13\mu\text{K}$ for the APM, $w_{TG} = 0.26 \pm 0.13\mu\text{K}$ for the *SDSS all* and $w_{TG} = 0.53 \pm 0.21\mu\text{K}$ for the *SDSS high-z* sample, in all cases we give 1- σ errorbars. We find the largest significance in the CMB-galaxy correlation for the *SDSS high-z* sample: $\Delta\chi^2 = 9.1$ (ie probability, $P = 0.3\%$ of no detection) for $\theta < 10^\circ$. In order to derive the significance levels for the ISW and SZ effects from the observed CMB-Galaxy correlations, we shall first discuss model predictions.

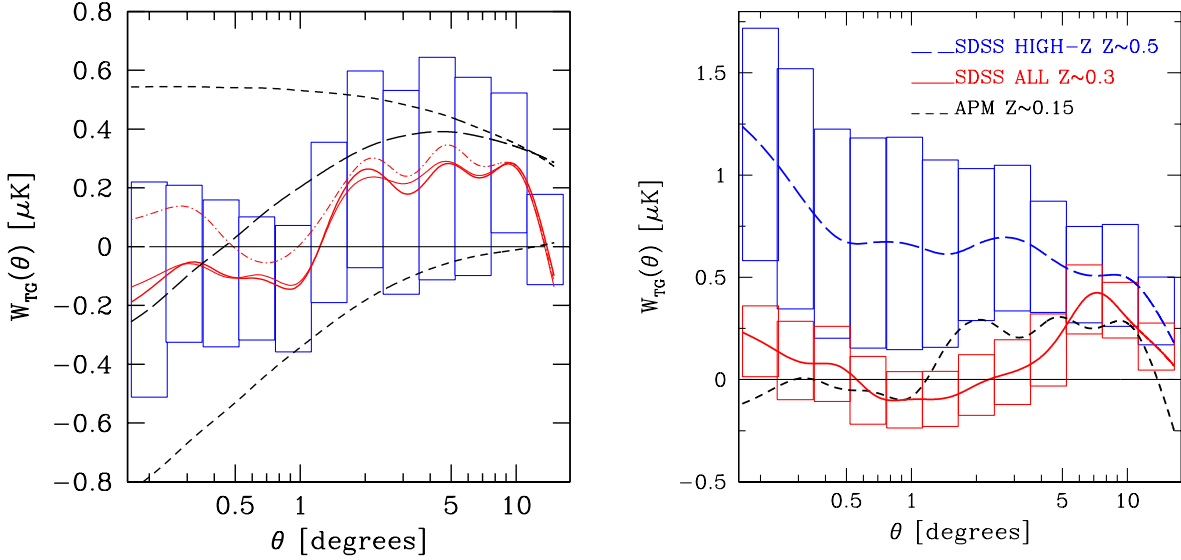


Figure 2: **(Left)** WMAP-APM correlation: the two solid lines and the dotted line show w_{TG} results for WMAP bands V, W, and the foreground “cleaned” map. Boxes show the 68% confidence levels. Also shown are the theoretical predictions for ISW and SZ (upper and lower short-dashed lines) and their sum (long-dashed line) for the best-fit Λ CDM model. **(Right)** WMAP-SDSS correlation: long dashed-line shows the measurement for the *SDSS HIGH-Z* sample, while the solid line displays the correlation for the *SDSS ALL* sample. For reference, short-dashed line displays the same measurement using the APM galaxy survey (see left panel) instead of SDSS.

4 Comparison to Theoretical Predictions

Photons coming to the observer from a given direction in the sky $\hat{\mathbf{n}}$ suffer an ISW temperature change given by: $\Delta T^{ISW}(\hat{\mathbf{n}}) = -2 \int dz \dot{\Phi}(\hat{\mathbf{n}}, z)$, and for a flat universe $\nabla^2 \Phi = -4\pi G a^2 \rho_m \delta$. In Fourier space it reads, $\Phi(k, z) = -3/2\Omega_m (H_0/k)^2 \delta(k, z)/a$, and thus:

$$w_{TG}^{ISW}(\theta) = \langle \Delta_T^{ISW} \delta_G \rangle = \int \frac{dk}{k} P(k) g(k\theta) \quad (1)$$

being, $g(k\theta) = 1/2\pi \int dz W_{ISW}(z) W_G(z) j_0(k\theta r)$, where the ISW window function is given by $W_{ISW} = -3\Omega_m (H_0/c)^2 \dot{F}(z)$, with $c/H_0 \simeq 3000h \text{ Mpc}^{-1}$, $\dot{F} = d(D/a)/dr = (H/c)D(f-1)$, and $f \simeq \Omega_m^{6/11}(z)$ quantifies the time evolution of the gravitational potential. The galaxy window function is $W_G \simeq b(z) D(z) \phi_G(z)$, which depends on the galaxy bias, linear dark-matter growth and the galaxy selection function. The ISW predictions for the 3 samples are shown in bottom panel of Fig.3. Unless stated otherwise, we use the concordance Λ CDM model with $\Omega_m = 0.3$, $\Omega_\Lambda = 0.7$, $\Gamma \simeq h\Omega_m = 0.2$ and $\sigma_8 = 1$.

For the thermal Sunyaev-Zeldovich (SZ) effect, we assume that the gas pressure δ_{gas} fluctuations are traced by the galaxy fluctuations $\delta_{gas} \simeq b_{gas} \delta_G$ with a relative amplitude given by the gas bias, $b_{gas} \simeq 2$, representative of galaxy clusters. A simple estimate of the SZ effect is thus²⁰,

$$w_{TG}^{SZ}(\theta) = -b_{gas} \overline{\Delta T} w_{GG}(\theta) \quad (2)$$

where $\overline{\Delta T} = j(x)\bar{y} T_0$, is the mean temperature change in CMB photons Compton scattered by electrons in hot intracluster gas, $T_0 \simeq 2.73\text{K}$ is the mean CMB temperature, $\bar{y} \simeq 1 \times 10^{-6}$ is the mean Compton parameter induced by galaxy clusters estimated for our samples, and $j(x) = -4.94$ is the negative SZ spectral factor for the V-band. The weak lensing effect prediction is quite similar to the ISW, we just need to replace the time derivative of the Newtonian potential by its 2D Laplacian²³: $W_{Lens} = 3k^2\Omega_m (H_0/c)^2 (D/a)/d(r)$, $d(r)$ being the angular distance to

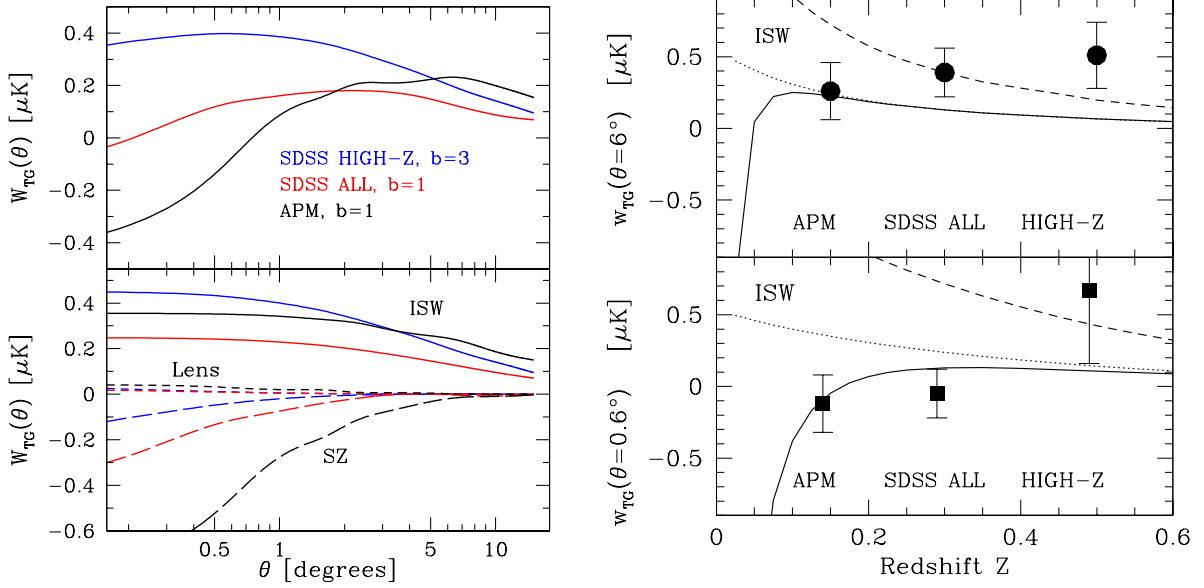


Figure 3: **(Left)** Theoretical predictions: (Bottom panel) Continuous, long and short dashed lines show the ISW, SZ and lensing predictions. Different sets of lines correspond to the APM (black), *SDSS all* (red) and *SDSS high-z* (blue) samples. (Top panel) The total prediction (ISW+SZ+Lensing) for the 3 samples. We have assumed a Λ CDM model with a fixed $b_{gas} = 2$ in all cases, $b = 3$ for *SDSS high-z* and $b = 1$ for APM and *SDSS all*. **(Right)** Predictions and measurements as a function of redshift: squares and circles correspond to measured cross-correlation at $\theta = 0.6^\circ$ and $\theta = 6^\circ$ respectively. Continuous lines show the corresponding SZ+ISW+lens predictions for $b = 1$ and $b_{gas} = 2$. Dotted and dashed lines shows the ISW with $b = 1$ and $b = 3$.

the lensing sources. The total predicted correlation is thus the sum of three terms: the ISW, thermal SZ and Lensing contributions, $w_{TG} = w_{TG}^{ISW} + w_{TG}^{SZ} + w_{TG}^{Lens}$. Fig.3 shows individual contributions of these effects (bottom panel) and the total (top) for the 3 samples analyzed. The ISW effect typically dominates for angles $\theta > 4^\circ$, while the SZ effect is expected to be significant on small scales $\theta < 1^\circ$. Lensing is found to be negligible at all scales for our samples.

Before one can make a direct comparison between theory and observations, the issue of galaxy bias must be addressed. As shown in Fig 3 (see plot on the right), the higher (*SDSS*) redshift sample requires a high bias $b > 1$ to explain the large cross-correlation seen at all scales. At low redshifts the measured correlation is dominated by the thermal SZ on small scales $\theta < 1^\circ$, while the ISW still dominates on large-scales, $\theta > 4^\circ$. Here no bias is required to reproduce the observations. Actually, this agrees quite well with our self-consistent bias estimation: for each sample we estimate the ratio $b^2 = w_{GG}/w_{MM}$, where w_{MM} and w_{GG} are the (theoretically predicted) matter and (measured) galaxy auto-correlation functions. For APM and *SDSS all* samples we find $b^2 \simeq 1$, while for the *SDSS high-z* sample we get $b^2 \simeq 6$.

4.1 Significance Tests

ISW effect: On large scales $\theta > 4^\circ$, the ISW effect is expected to dominate for all survey depths (see Fig 3). Therefore, from the large-angle CMB-Galaxy correlation, we can directly infer the ISW effect (ie, $w_{TG} = w_{TG}^{ISW}$, see end of §3). In particular, for the APM survey, a constant correlation fit rejects the null detection with high significance $\Delta\chi^2 = 6.0$ ($P = 1.4\%$), similar to the values for the *SDSS high-z* sample $\Delta\chi^2 = 6.1$ ($P = 1.3\%$). A smaller significance is obtained from the *SDSS all* sources: $\Delta\chi^2 = 3.9$ ($P = 4.8\%$). Since these samples are basically independent, we can combine them to infer a total significance for the ISW detection: we find a total $\Delta\chi^2 = 16$ ($P = 0.1\%$ for 3 d.o.f) corresponding to a 3.3σ . Note we could do better using a (scale dependent) Λ CDM model theory prediction, but at the cost of introducing model

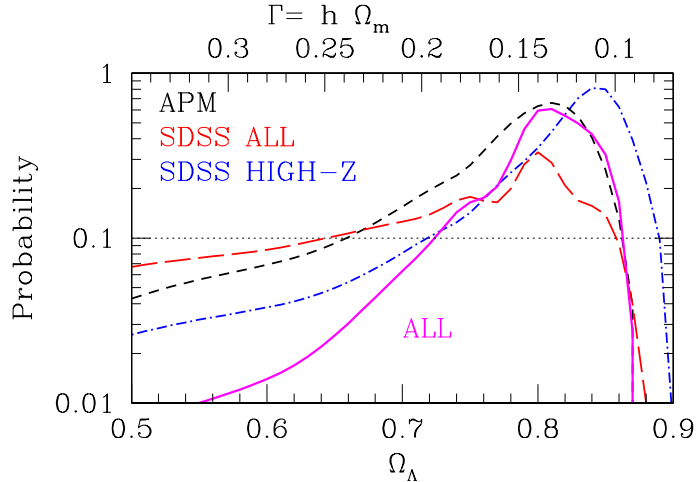


Figure 4: Estimating dark-energy: Long-dashed, short-dashed and dot-dashed lines show the probability distribution for Ω_Λ in the *SDSS all*, APM and *SDSS high-z* samples. Solid line shows the combined distribution.

dependent detection levels. Moreover, we can further include the ISW-dominated small angle bins in our deepest sample, where SZ is negligible, increasing the significance to $\Delta\chi^2 = 18.8$, ($P = 0.03\%$ for 3 d.o.f.), ie we detect the ISW effect at the a 3.6σ level.

SZ effect: We can estimate the significance of the drop in the signal at small angles in the APM and *SDSS all* samples due to the SZ effect (see Fig3) using the best-fit constant at large angles (ie, the ISW signal) and ask for the observed deviation from such value at smaller scales. For $\theta < 1^\circ$, we find: $w_{TG}^{SZ} = -0.41 \pm 0.16$ for APM, and $w_{TG}^{SZ} = -0.27 \pm 0.11$ for *SDSS all* ($1\text{-}\sigma$ errorbars). This test gives $\Delta\chi^2 = 8.5$ ($P = 0.3\%$) for the APM sample and $\Delta\chi^2 = 5.5$ ($P = 2\%$) for the *SDSS all*.

5 Discussion

We have cross-correlated WMAP with the APM and SDSS DR1 optical galaxy surveys. Our analysis includes 5800 deg^2 (14 % of the sky) and comprises 7.6 million galaxies in compact regions of the north and south hemispheres. We obtain significant cross-correlations for galaxy samples in a wide redshift range ($z \sim 0.15 - 0.5$). We detect a positive large-scale correlation which is in good agreement with the ISW effect and its redshift evolution as expected from Λ CDM models. The combined analysis for the 3 samples investigated (APM, SDSS-all and SDSS high-z) yields a 99.97% ISW detection level (3.6σ).

Before using matter predictions to estimate parameters from the observed CMB-galaxy correlation, we self-consistently estimated the galaxy bias b by comparing the matter angular auto-correlation function in each model to the measured galaxy auto-correlation in each sample.

Once galaxy bias is determined, we find that all the measured cross-correlations on large scales are in good agreement with ISW predictions for a dark-energy dominated universe. Fig 4 shows the probability distribution for Ω_Λ in a flat Λ CDM model. We have fixed $\sigma_8 = 1$, $h = 0.7$ and $\Omega_M + \Omega_\Lambda = 1$. As we vary Ω_Λ the shape parameter for the linear power spectrum $P(k)$ consistently changes $\Gamma = h\Omega_M$. We only use the data for $\theta > 4^\circ$, where the ISW is the dominant contribution for all samples.

From our analysis a coherent dark-energy dominated universe arises: both APM and SDSS samples point to large values of Ω_Λ , with the best fit $\Omega_\Lambda \simeq 0.8$ and a rather narrow 2σ range $\Omega_\Lambda = 0.69 - 0.87$. We stress that this dark-energy estimation is independent from other known probes (e.g, SN type Ia data).

We have also found evidence for the thermal SZ effect from the drop of the CMB-galaxy correlation on small-scales in the low- z samples of APM and SDSS galaxies. The estimated SZ effect is compatible with a Compton parameter $\bar{y} \simeq 1 \times 10^{-6}$. These new measurements can be used to constrain the redshift evolution of the physical properties of gas inside galaxy clusters.

Upcoming wider and deeper Galaxy surveys (e.g future data releases from the SDSS) in combination with higher-spatial resolution and sensitivity full-sky CMB maps (e.g. 2yr-WMAP data, PLANCK) shall eventually allow for a higher significance detection of both the ISW and SZ signals. Moreover these new generation surveys can potentially extract the challenging lensing signal on large-scales^{23,12,14}. This program will eventually provide us with a better understanding of the gravitational instability picture and set new and tighter constraints on basic cosmological parameters.

Acknowledgments

We acknowledge support from the Barcelona-Paris bilateral project (Picasso Programme). PF acknowledges support from a post-doctoral CMBNet fellowship from the EC and grant NASA ATP NAG5-12101. EG and FJC acknowledge the Spanish MCyT, project AYA2002-00850, EC-FEDER funding.

References

1. Afshordi, N., Loh, Y.-S., Strauss, M.A., 2003, astro-ph/0308260
2. Abazajian, K., et al. 2003, AJ, submitted, astro-ph/0305492
3. Bennett, C.L., et al. 2003, ApJ.Suppl., 148, 1
4. Boughn, S.P. & Crittenden, R.G. 2003, astro-ph/0305001
5. Crittenden, R.G., Turok, N., 1996, Phys.Rev.Lett., 76, 575
6. Diego, J., Silk, J., Sliwa, W., 2003, astro-ph/0302268
7. Fosalba, P. & Gaztañaga, E., 2003, astro-ph/0305468
8. Fosalba, P., Gaztañaga, E., Castander, F.J., 2003, ApJ.Lett. accepted, astro-ph/0307249
9. Górski, K.M., Hivon, E., & Wandelt, B.D. 1999, in Proc.MPA-ESO Conf., Evolution of Large-Scale Structure: From Recombination to Garching, p.37, Ed. A.J.Banday, R.K.Seth, & L.A.N da Costa (Enschede: PrintPartners Ipskamp)
10. Hernandez-Monteagudo, C. & Rubino-Martin, J.A., 2003, astro-ph/0305606
11. Hinshaw, G.F. et al. 2003, astro-ph/0302222
12. Hu, W., 2002, PRD, 65, 23003
13. Hu, W. & Dodelson, S., 2002, An.Rev.Astron.Astrophys., 40, 171
14. Kesden, M., Kamionkowski M., Cooray, A., 2003, astro-ph/0306597
15. Kofman, L.A., Starobinsky, A.A., 1985, Sov. Astron. Lett. 11, 271
16. Maddox, S.J., et al. 1990, MNRAS, 242, 43
17. Myers, A.D., et al. 2003, astro-ph/0306180
18. Nolta, M.R., et al. 2003, astro-ph/0305097
19. Peiris, H., Spergel, D.N., 2000, ApJ, 540, 605
20. Refregier, A., Spergel D.N., Herbig T., 2000, ApJ, 531, 31
21. Sachs, R.K. & Wolfe, A.M. 1967, ApJ, 147, 73
22. Scranton, R., et al. 2003, astro-ph/0307335
23. Seljak, U., 1996, ApJ, 463, 1
24. Sunyaev, R.A. & Zeldovich, I.B., 1980, An.Rev.Astron.Astrophys., 18, 537
25. Tegmark, M., et al. 2003, astro-ph/0302496